TJ21.3

Statistical Estimation of a 13.3 micron Channel for VIIRS using Multisensor Data Fusion with Application to Cloud-Top Pressure Estimation

Irina Gladkova[1], James Cross III[2], Paul Menzel[3], Andrew Heidinger[4], and Michael Grossberg[1]

[1]City College of New York, NOAA/CREST
[2]The Graduate Center, CUNY
[3]CIMSS/Univ. of Wisconsin
[4]NOAA/NESDIS/STAR

Abstract

Meteorologists and other scientists rely heavily on remotely sensed data collected from instruments aboard orbiting satellites. The design of such instruments requires technical and economic trade-offs that results in certain desirable data not being directly available. One way to mitigate the lack of availability of this data is to use machine learning techniques to estimate the values that cannot be directly observed. This can be accomplished by exploiting statistical correlation with information in available data sets. By combining the information from multiple other sources it is often possible to create an accurate estimate of the physical parameters which are not directly observed. We apply this idea toward the problem of estimating the 13.3μm band for the Visible Infrared Imaging Radiometer Suite (VIIRS), an instrument aboard NOAA's operational satellite, Suomi NPP. The radiance from the 13.3μm band is not directly available from VIIRS although this band has important applications such as estimating cloud-top pressure. We demonstrate that a reliable estimate of this band can be made using other VIIRS bands at 4, 9, 11 and 12μm, as well as input from the Cross-track Infrared Sounder (CrIS), which produces data at much finer spectral resolution, making measurements in hundreds of nearby infrared bands, though with lower spatial resolution. We have tested the result as input values to an algorithm which estimates cloud top pressure using data from 11, 12, and 13.3μm bands.

1 Introduction

Clouds remain a subject in climate studies because of their dominant role in Earth's energy balance and water cycle. Cloud visible reflectivity and infrared trapping have significant impact on weather systems and climate changes. Among the challenges are to better describe the horizontal and vertical variability of global cloud properties and to mitigate problems in long-term descriptions of cloud trends caused by sensor changes from Polar-Orbiting Environmental Satellite (POES) to Earth Observing System (EOS) to Joint Polar Satellite System (JPSS) platforms. With the October 2011 launch of the Suomi National Polar Partnership (SNPP), the Visible and Infrared Imaging Radiometer Suite (VIIRS) becomes the operational imager for the afternoon NOAA environmental polar orbiting satellite. Additionally, the Cross-track Infrared Sounder (CrIS), which is a Fourier transform spectrometer, becomes the operational sounder. VIIRS and CrIS are intended to continue the measurements and products established with Advanced Very High Resolution Radiometer (AVHRR) and HIRS (High resolution Infrared Radiometer Sounder) sensors that have flown on NOAA POES platforms for over 30 years. In addition the climate measurements started with the MODerate resolution Imaging Spectroradiometer (MODIS) and the Advanced Infrared Sounder (AIRS) in the NASA research EOS are also to be continued [4, 1].

However, VIIRS does not have any spectral bands located in H_2O or CO_2 absorption bands, which degrades its ability to determine semi-transparent cloud properties (including cloud top pressures/heights) compared to that of sensors including even a single absorption channel [3]. In an effort to ensure continuity and consistency between

historical cloud products and those provided from the SNPP sensors (and JPSS in the future), we demonstrate a VIIRS plus CrIS cloud algorithm that can extend the AVHRR/HIRS and MODIS/AIRS cloud record. VIIRS has 16 spectral bands measured at 780 meter resolution at nadir, 9 in the visible and near infrared plus 5 in the infrared. This paper presents a technique to generate an additional VIIRS channel at 13.3μm statistically constructed from CrIS and VIIRS measurements. The CrIS sensor makes 1305 high spectral resolution measurements from 15.1 to 3.8μm at 15 km resolution; the measurements in the 15μm CO_2 absorption bands are especially important for cloud property retrieval. Using the infrared spectral bands on VIIRS at 780 meter resolution and a convolution of the 15μm spectral measurements on CrIS at 15 km resolution, an artificial 13.3μm channel at 780 meter resolution is created using by statistical estimation. The observed VIIRS channels combined with the statistically constructed 13.3μm channel are then used in a cloud top pressure algorithm that has been developed for the pending Advanced Baseline Imager to be launched in 2015 on GOES-R [2].

As proxy for VIIRS we can use data from the Moderate Resolution Image Spectroradiometer (MODIS), an instrument aboard the NASA satellites Aqua and Terra, part of the Earth Observing System (EOS). This instrument has bands that match those of VIIRS. In particular, MODIS bands 23, 29, 31, and 32 (4, 8.5, 11, and 12μm) have characteristics similar to the M13, M14, M15 and M16 bands of VIIRS. In addition, MODIS band 33 is centered at 13.3μm, which is the target spectral band, and has all of the resolution, location, and temporal characteristics desired. To stand in for the CrIS component, we will use data from the Atmospheric Infrared Sounder (AIRS), which is also aboard the Aqua satellite. Like CrIS, AIRS covers the target spectral response range around 13.3μm (through a multitude of narrow bands), and like CrIS at a much lower spatial resolution.

There are several different families of techniques for achieving the unification of related data from different sources generally called image or data fusion [6]. The major purpose of those studies has been to generate high-resolution multispectral imagery combining the spectral characteristics of low-resolution data with the high spatial resolution of the panchromatic imagery. As a class, these methods are known as pan-sharpening algorithms. A number of approaches to this problem have been developed with varying assumptions, and a review of pan-sharpening data fusion methods can be found in [10]. Most common are IHS (Intensity-Hue-Saturation) Transform [11, 12], Brovey Transform [13, 14], High-Pass Filtering [15, 16], High-Pass Modulation [17], Principal Component Analysis [18], ARSIS [19], À Trous Algorithm (Wavelet Based Transform) [20, 21, 22, 23], Mallat algorithms (Wavelet-based image fusion methods) [24, 25, 26, 27, 28, 29]. All of these data fusion methods operate on the assumption of having geo-rectified data under clear sky and captured at the same time. There have also been a few attempts to apply fusion tools to land surface modelling. For example, surface reflectance was modelled to fuse Landsat and MODIS measurements via the spatial and temporal adaptive reflectance fusion model (STARFM) for clear sky conditions [30, 31, 32].

Estimation of VIIRS 13.3μm band fits into the general image fusion framework as defined in [6], but does not fit into the framework of pan-sharpening fusion algorithms. Wald (c.f. [6]) defines image fusion as "a formal framework in which are expressed means and tools for the alliance of data originating from different sources. It aims at obtaining information of a greater quality, although the exact definition of 'greater quality' will depend on the application." According to Wald, the quality assessment depends on the application. In this case the synthetic 13.3μm band is intended to be used in algorithms to create data products, such as the cloud-top pressure product described below, in place of a measured band which is not available. Thus the assessment of the quality of a synthetic band is the accuracy of derived products using the estimated data. Fortunately there are opportunities to make quantitative assessments of such an approach through the use of MODIS and AIRS as proxy data sources, since in the case of MODIS, unlike with VIIRS, a directly measured 13.3μm band *is* available. The results of preliminary tests are described in Section 3.

We will assume in this work that the value at a point of the the target 13.3μm can be estimated as a function of bands available on VIIRS, at least locally. We will show that this assumption approximately holds by testing it with a representative set of MODIS and AIRS granules as a proxy for VIIRS and CrIS. In addition, to compute the function which produces 13.3μm estimated values, we will assume a measure of scale-invariance in the relationship between available source bands and the target band. This assumption makes it possible to establish a relationship between a vector of radiance values in the source bands and the scalar radiance value in the target band for low resolution images, and apply the relationship to high resolution images. We will provide some evidence for the validity of this assumption as well.

The remainder of this paper is organized as follows. Section 2 describes the estimation algorithm in detail. Section 3 analyzes the results of applying the algorithm

to representative sets of overlapping MODIS and AIRS granules and describes the results of using the artificial 13.3μm band in the generation of cloud-top pressure, a real-world data product with important meteorological applications. Section 4 presents the results when the multisensory fusion approach is applied to VIIRS and CrIS granules, also showing a comparison with nearly coincident MODIS results. The paper is concluded in Section 5.

2 Statistical Estimation

In this section we will briefly describe the statistical estimation algorithm for estimating the high spatial resolution radiance values from a collection of low resolution hyperspectral images measured around the desired wavelength by a hyperspectral instrument and a collection of high spatial resolution images measured by low spectral resolution instrument at a few other (not necessarily neighbouring) wavelengths. The block diagram of the estimation algorithm is shown in Figure 1. The top left of the diagram indicates the flow of corresponding geometric information for VIIRS and hyperspectral instrument (CrIS) which is used to average high resolution VIIRS images R^H_ν for the input bands $\nu = (\nu_1, \nu_2, \cdots, \nu_n)$, to produce simulated low resolution bands R^L_ν, matching the resolution of CrIS. On the top right of the diagram in Figure 1, the flow indicates that a 13.3μm target band at CrIS resolution is estimated using the desired spectral response from the CrIS radiances, and the result is denoted R^L_λ. The key element of this work is that we introduce a spatially varying estimator F which minimizes the mean square error

$$|\tilde{R}^L_\lambda - F(R^L_\nu)|^2.$$

The function F is a function of location and input band radiances at each pixel. By assuming that the relationship of pointwise radiances holds invariant of scale, we can produce an estimate $\tilde{R}^H_\lambda = F(R^H_\nu)$ of the true 13.3μm target band radiances 13.3μm at the higher VIIRS resultion using the high resolution VIIRS measured input radiances $F(R^H_\nu)$ as shown in the lower right of the block diagram. Figure 2 (left side) shows the spectral response we used to create the low resolution 13.3μm band from AIRS (CrIS proxy) shown on the top right. Figure 3 shows the four input bands – 4, 8.5, 11, and 12μm (MODIS bands 23, 29, 31, and 32 at AIRS resolution) used for building the 13.3μm band estimator, F. The bands were produced by averaging the MODIS bands using the AIRS geometry and pixel footprints.

A meaningful assertion that 13.3μm values can be computed from a function F of the four input bands, implies that the local variance of the values 13.3μm should be small in a neighbourhood of a fixed value for the input bands. In this case we are using MODIS data exclusively since for this instrument, the measured 13.3μm values are known. Visualizing this as a scatter plot would require 1 output and 4 input, or a total of 5 dimensions. To create a 3-D visualization we have taken the x-y plane to be projections into the first 2 PCA components of the input variables, for figure 4, with the z-axis being the corresponding value in the 13.3μm band. The figure shows two rotated views of this scatter plot. It is clear from the figure that, indeed, the relationship of the input bands to the target band is essentially a function.

The estimation function is implemented using a k-nearest neighbour search, and locally averaging the results. In particular, to estimate the target radiance at a given pixel, the corresponding vector of radiance values for the source bands at high resolution is used to query the database. The query is efficiently executed using the k-d tree data search algorithm to find k-nearest neighbours. The corresponding target 13.3μm values for these neighbours are then averaged to create an estimated value for each pixel at the higher resolution in the target band 13.3μm band.

3 Fusion Results: MODIS/AIRS as proxy

To evaluate our algorithm we require ground truth values R^H_λ since the error of our estimates are given by the mean square errors $|R^H_\lambda - \tilde{R}^H|^2$. Since the 13.3$\mu$m values are unavailable for VIIRS, we use MODIS images as a proxy for VIIRS, and AIRS hyperspectral data as a proxy for CrIS hyperspectral data. In this section we will demonstrate two examples of our statistical estimation of a 13.3μm channel in which MODIS/AIRS pair is used as proxy for VIIRS/CrIS. The first example is based on MODIS granule MYD021KM.A2012020.0500 and AIRS.2012.01.20.050, a cloudy ocean scene off the southern coast of Australia. Figure 5 demonstrates the results of applying the algorithm to these granules. The actual radiances for MODIS 13.3μm band are shown on the right, the estimated values produced by the algorithm are in the center, and the absolute value of the difference image is on the left.

Figure 6 shows the results for MODIS Aqua granule MYD021KM.A2012243.0440, a recent granule situated over the Korean Peninsula, and two AIRS L1B granules which overlap it, AIRS.2012.08.30.046 and AIRS.2012.08.30.047. Once again, the actual and esti-

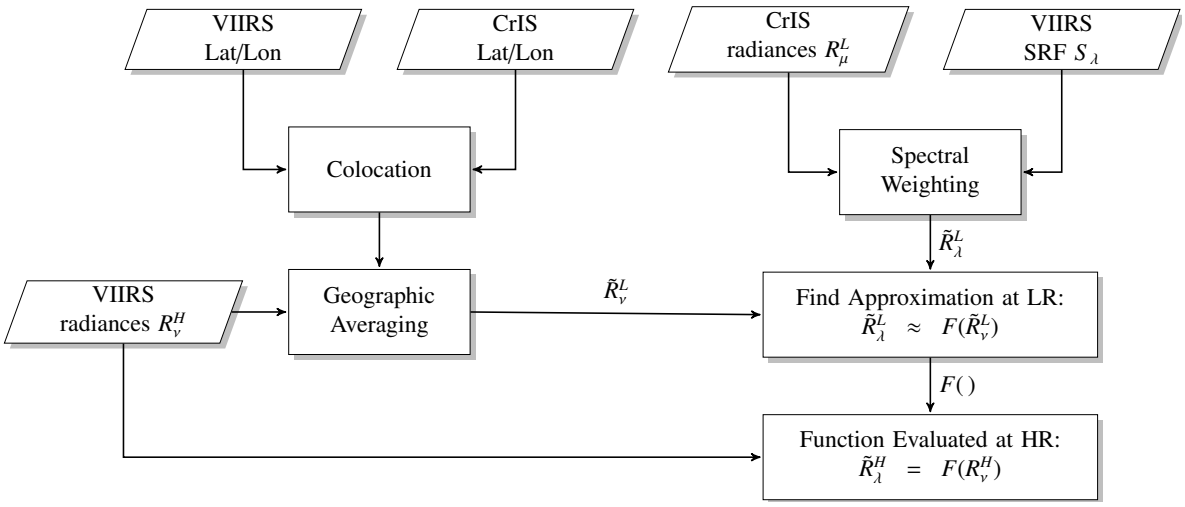

Figure 1: Block diagram of statistical estimation algorithm.

mated high-resolution 13.3μm band, in the left and center respectively, are very similar. The image on the right shows that the difference is very small. Histograms of the differences between actual 13.3μm band and the estimated values are shown in Figure 7.

In addition to testing the 13.3μm values produced by our estimation against the known MODIS 13.3μm band, we tested it as input values to an algorithm which estimates cloud top pressure using data from 11, 12, and 13.3μm bands (cf. Figures 8 and 9). This algorithm was developed for the Geostationary Operational Environmental Satellite R Series (GOES-R). That satellite will be launched as soon as 2015 and will carry the Advanced Baseline Imager (ABI) which will measure 13.3μm band (though at a lower 2km spatial resolution). These tests showed that similarly-synthesized data from VIIRS and CrIS would allow VIIRS/CrIS to match GOES-R in terms of cloud-top pressure determination, to within the GOES-R specifications, which is especially important for getting such values for night scenes since GOES-R, unlike VIIRS, relies on data in the visible to near-infrared range.

4 Fusion Results: VIIRS/CrIS

In this section we pursue the statistical estimation of a 13.3 micron channel for VIIRS data using the collocated CrIS measurements. As in the previous section, we convolve the CrIS high spectral resolution measurements with the MODIS channel 33 spectral response function to create broadband 13.3 micron measurements at CrIS resolution. Then a regression relationship is made between those measurements and spatially collocated VIIRS M13, M14, M15, and M16 measurements aggregated to CrIS spatial resolution. Thereafter that regression relationship is applied to full resolution VIIRS 780 meter measurements to achieve statistically estimated VIIRS 13.3 micron spectral band measurements.

Figure 11 shows a comparison of VIIRS 13.3 micron brightness temperatures statistically constructed using Suomi NPP radiance data from 28 August 2012 over Korea and MODIS brightness temperatures from Aqua 10 minutes earlier. There is excellent agreement in the synoptic scale patterns. Figure 12 displays the cloud top pressures derived from the MODIS radiances using the ABI algorithm along with the same for VIIRS with the statistically estimated 13.3 micron radiances. Again the overall agreement in this level 2 parameter for the two scenes separated by ten minutes is very good.

To investigate the impact of the 13.3 micron radiances, Figure 13 (left) shows the cloud top pressures derived without the 13.3 micron data using an optimal estimation approach that relies on the NCEP Global Data Assimilation System as a first guess. The difference of with and without 13.3 micron data is shown in Figure 13 (right). In high thin cirrus west of North Korea, the ABI algorithm with the 13.3 micron data gets the CTP at 250 hPa while the VIIRS optimal estimation without the 13.3 micron data pins it at the tropopause. In low clouds over the Pacific Ocean south of Japan, the 13.3 micron data helps the ABI algorithm left the clouds off the ocean surface, in better agreement with MODIS results.

5 Conclusion

With preliminary examples using both Aqua MODIS and AIRS data as well as Suomi NPP VIIRS and CrIS data, we demonstrate that a reliable estimate of the imager 13.3 micron broadband radiance data can be statistically estimated from the sounder high spectral resolution infrared data guided by the imager spectral band radiances at 4, 8.6, 11 and 12 microns. We have successfully tested the resulting data as input values to an algorithm which estimates cloud top pressure using data from 11, 12, and 13.3 micron bands; we find good agreement between VIIRS and MODIS cloud top pressures when VIIRS has the assistance from the estimated 13.3 micron channel. These example results suggest that synergistic use of VIIRS and CrIS measurements can overcome the absence of a 13.3 micron channel on VIIRS. Routine application of this multisensor fusion approach should be investigated further.

References

[1] Aumann, H. H., M. T. Chahine, C. Gautier, M. D. Goldberg, E. Kalnay, L. M. McMillan, H. Revercomb, P. W. Rosenkranz, W. L. Smith, D. H. Staelin, L. L. Strow, and J. Susskind, 2003: AIRS/AMSU/HSB on the Aqua mission: Design, science objective, data products, and processing systems, IEEE Trans. Geosci. Remote Sens., 41, 253-264.

[2] Heidinger, Andrew K, 2011: ABI Cloud Height Algorithm (ACHA) Algorithm Theoretical Basis Document (ATBD), GOES-R Program Office. (http://www.goes-r.gov/products/ATBDs/baseline/Cloud_CldHeight_v2.0_no_color.pdf)

[3] Heidinger, A. K., M. J. Pavolonis, R. E. Holz, B. A. Baum, and S. Berthier, 2010: Using CALIPSO to explore the sensitivity to cirrus height in the infrared observations from NPOESS/VIIRS and GOES-R/ABI. J. Geophys. Res., 115.

[4] King, M. D., Y. J. Kaufman, W. P. Menzel, and D. Tanre, 1992: Remote Sensing of Cloud, Aerosol and Water Vapor Properties from the Moderate Resolution Imaging Spectrometer (MODIS). IEEE Trans. and Geosci. and Remote Sensing, 30, 2-27.

[5] Wong, E., Hutchison, K.D., Ou, S.C., and K. N. Liou, 2007: Cirrus cloud top temperatures retrieved from radiances in the National Polar-Orbiting Operational Environmental Satellite System-Visible Infrared Imager Radiometer Suite 8.55 and 12.0 m bandpasses, Appl. Opt., 46, 1316-1325.

[6] L. Wald 1999: Some Terms of Reference in Data Fusion, IEEE Transactions on Geoscience and Remote Sensing, Vol. 37, No. 3, 1190–1193

[7] L. Wald, T. Ranchin, and M. Mangolini 1997: Fusion of satellite images of different spatial resolutions: Assessing the quality of resulting images, Photogramm. Eng. Remote Sens., vol. 63, no. 6, pp. 691699.

[8] J. Li 2000: Spatial quality evaluation of fusion of different resolution images, ISPRS Int. Arch. Photogramm. Remote Sens., vol. 33, no. B2-2, pp. 339 346.

[9] C. Thomas and L. Wald, Assessment of the quality of fused products, in Proc. 24th EARSeL Annu. Symp. New Strategies Eur. Remote Sens., Dubrovnik, Croatia, May 2527, 2004. M. Oluic, Ed., Rotterdam, The Netherlands: Balkema, 2005, pp. 317325.

[10] C. Thomas, T. Ranchin, L. Wald, and J Chanussot 2008: Synthesis of Multispectral Images to High Spatial Resolution: A Critical Review of Fusion Methods Based on Remote Sensing Physics, IEEE Transactions on Geoscience and Remote Sensing,, Vol. 46, No. 5, pp. 1301–1312

[11] W. J. Carper, T. M. Lillesand, and R. W. Kiefer 1990: The use of Intensity-Hue-Saturation transform for merging SPOT panchromatic and multispectral image data, Photogramm. Eng. Remote Sens., vol. 56, no. 4, pp. 459-467

[12] T. M. Tu, S. C. Su, H. C. Shyu, and P. S. Huang 2001: A new look at IHS-like image fusion methods, Inf. Fusion, vol. 2, no. 3, pp. 177-186

[13] J. G. Liu 2000: Smoothing filter-based intensity modulation: A spectral preserve image fusion technique for improving spatial details, Int. J. Remote Sens., vol. 21, no. 18, pp. 3461-3472

[14] A. R. Gillespie, A. B. Kahle, and R. E. Walker 1987: Color enhancement of highly correlated images II. Channel ratio and chromaticity transformation techniques, Remote Sens. Environ., vol. 22, pp. 343-365

[15] R. A. Schowengerdt 1997: Remote Sensing: Models and Methods for Image Processing, 2nd ed. Orlando, FL: Academic

[16] S. de Bthune, F. Muller, and J. P. Donnay 1998: Fusion of multi-spectral and panchromatic images by local mean and variance matching filtering techniques, Fusion of Earth Data

[17] B. Aiazzi, L. Alparone, S. Baronti, and A. Garzelli 2002:Context-driven fusion of high spatial and spectral resolution images based on oversampled multi-resolution analysis, IEEE Trans. Geosci. Remote Sens., vol. 40, no. 10, pp. 2300-2312

[18] P. S. Chavez and A. Y. Kwarteng 1989: Extracting spectral contrast in Landsat Thematic Mapper image data using selective principle component analysis, Photogramm. Eng. Remote Sens., vol. 55, no. 3, pp. 339348

[19] T. Ranchin and L. Wald 2000: Fusion of high spatial and spectral resolution images: The ARSIS concept and its implementation, Photogramm. Eng. Remote Sens., vol. 66, no. 1, pp. 49-61

[20] M. J. Shensa 1992: The discrete wavelet transform:Wedding the Trous and Mallat algorithms, IEEE Trans. Signal Process., vol. 40, no. 10, pp. 2464-2482

[21] J. Nez, X. Otazu, O. Fors, A. Prades, V. Pal, and R. Arbiol 1999: Multiresolution- based image fusion with additive wavelet decomposition, IEEE Trans. Geosci. Remote Sens., vol. 37, no. 3, pp. 1204-1211

[22] B. Aiazzi, L. Alparone, S. Baronti, and A. Garzelli 2002: Context-driven fusion of high spatial and spectral resolution images based on oversampled multi-resolution analysis, IEEE Trans. Geosci. Remote Sens., vol. 40, no. 10, pp. 2300-2312

[23] F. Murtagh and J. L. Starck 2000: Image processing through multiscale analysis and measurement noise modeling, Stat. Comput., vol. 10, no. 2, pp. 95-103

[24] S. Mallat 1989: A theory for multi-resolution signal: The wavelet representation, IEEE Trans. Pattern Anal. Mach. Intell., vol. 11, no. 7, pp. 674-693

[25] J. Zhou, D. L. Civco, and J. A. Silander 1998: A wavelet transform method to merge Landsat TM and SPOT panchromatic data, Int. J. Remote Sens., vol. 19, no. 4, pp. 743-757

[26] D. A. Yocky 1995: Image merging and data fusion by means of the discrete two-dimensional wavelet transform, J. Opt. Soc. Amer. A, vol. 12, no. 9, pp. 1834-1841

[27] D. A. Yocky 1996: Multiresolution wavelet decomposition image merger of Landsat Thematic Mapper and SPOT Panchromatic data, Photogramm. Eng. Remote Sens., vol. 62, no. 9, pp. 1067-1074

[28] F. Murtagh and J. L. Starck 2000: Image processing through multiscale analysis and measurement noise modeling, Stat. Comput., vol. 10, no. 2, pp. 95-103

[29] J. Nez, X. Otazu, O. Fors, A. Prades, V. Pal, and R. Arbiol 1999: Multiresolution- based image fusion with additive wavelet decomposition, IEEE Trans. Geosci. Remote Sens., vol. 37, no. 3, pp. 1204-1211

[30] F. Gao, J. Masek, M. Schwaller, F. Hall 2006: On the Blending of the Landsat and MODIS Surface Reectance: Predicting Daily Landsat Surface Reectance, IEEE Trans. Geoscience and Remote Sensing, Vol.44, No.8, 2207–2218

[31] F. Gao, J. T. Morisette, R. E. Wolfe, G. Ederer, J. Pedelty, E. Masuoka, R. Myneni, B. Tan, J. Nightingale 2008: An Algorithm to Produce Temporally and Spatially Continuous MODIS-LAI Time Series, IEEE Trans. Geoscience and Remote Sensing, Vol.5, No.1, 60–64

[32] M. C. Anderson, W. P. Kustas, J. M. Norman, C. R. Hain, J. R. Mecikalski, L. Schultz, M. P. Gonzalez-Dugo, C. Cammalleri, G. dUrso, A. Pimstein, F. Gao 2010: Mapping daily evapotranspiration at eld to global scales using geostationary and polar orbiting satellite imagery, Hydrol. Earth Syst. Sci. Discuss., 7, 5957–5990

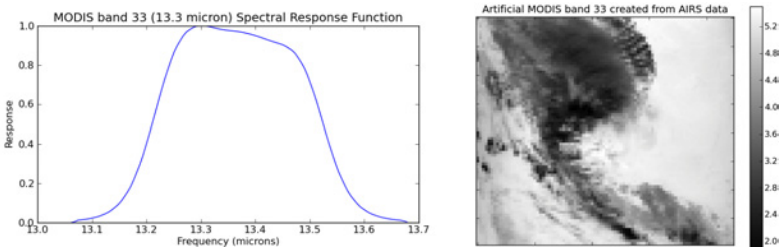

Figure 2: Spectral response function used to estimate the 13.3μm band from the hyperspectral image at lower resolution (left) and the estimated $\tilde{R}^L_\lambda$ used in the Estimation Block of the diagram as dependent variable (right).

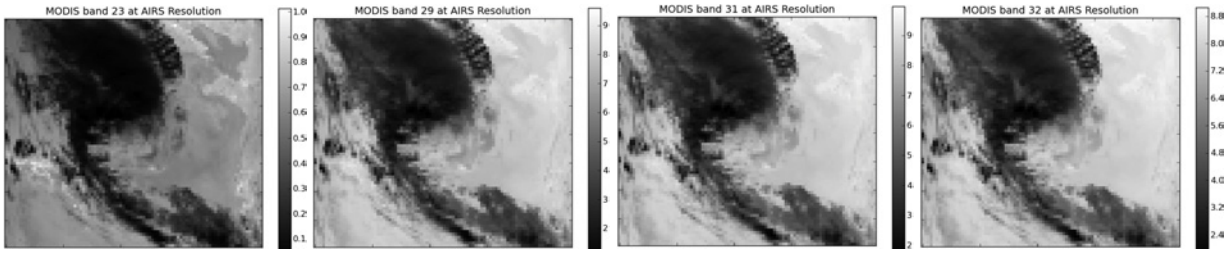

Figure 3: Lower spatial resolution radiance values $\tilde{R}^L_\nu$ computed from the known bands. The original available bands of MODIS were degraded to AIRS resolution using geographic collocation data and used in the Estimation Block of the diagram as independent variables.

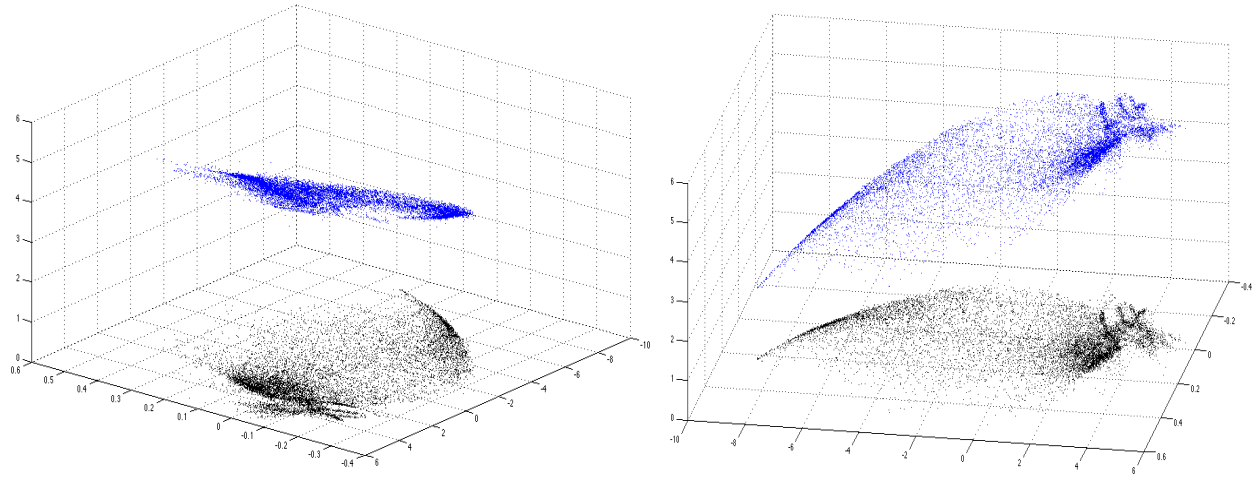

Figure 4: Scatter plot of the target 13.3μm band radiance values (from MODIS) (z-axis) as a function of the four input bands radiances projected into 2-PCA components (x-y plane) for visualization. The apparent surface of points is evidence that the target band can be well estimated as function of the input bands.

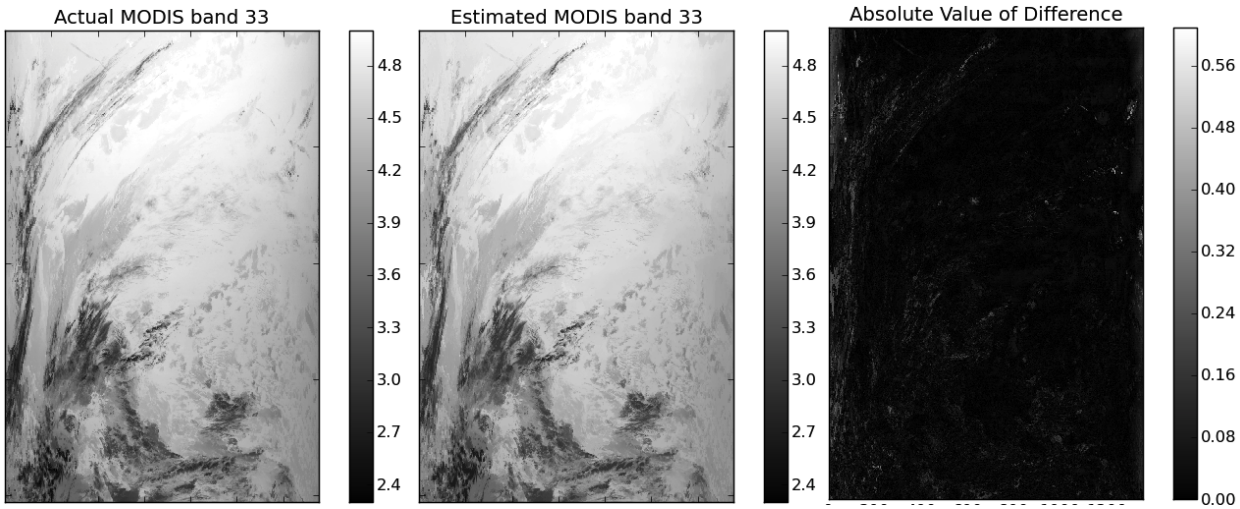

Figure 5: Actual (left), Estimated (middle), Magnitude of the difference (right)

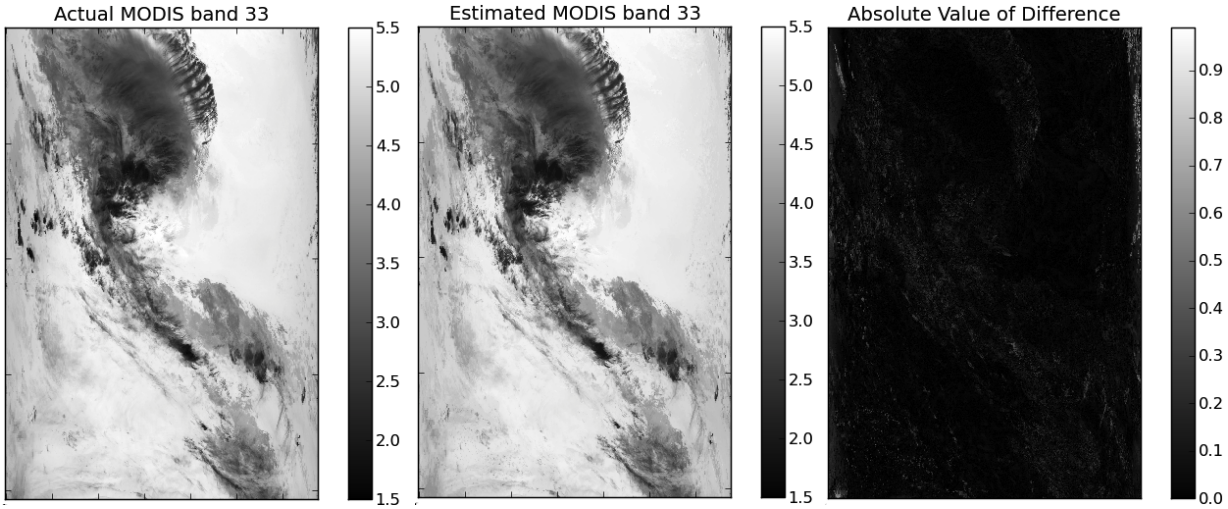

Figure 6: Actual (left), Estimated (middle), Magnitude of the difference (right).

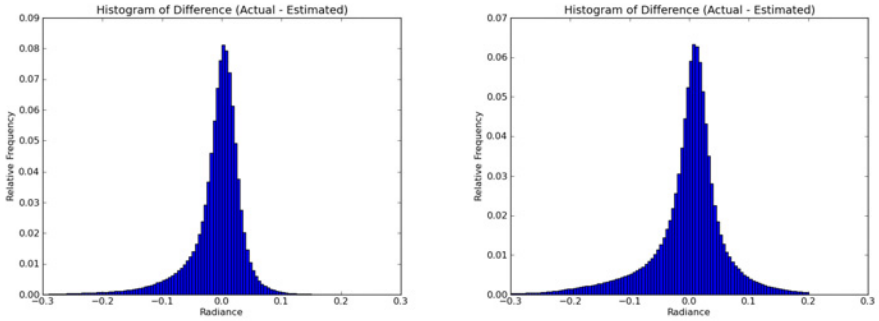

Figure 7: Histograms of the differences between actual 13.3 micron band and the estimated: Case 1 (left), Case 2 (right).

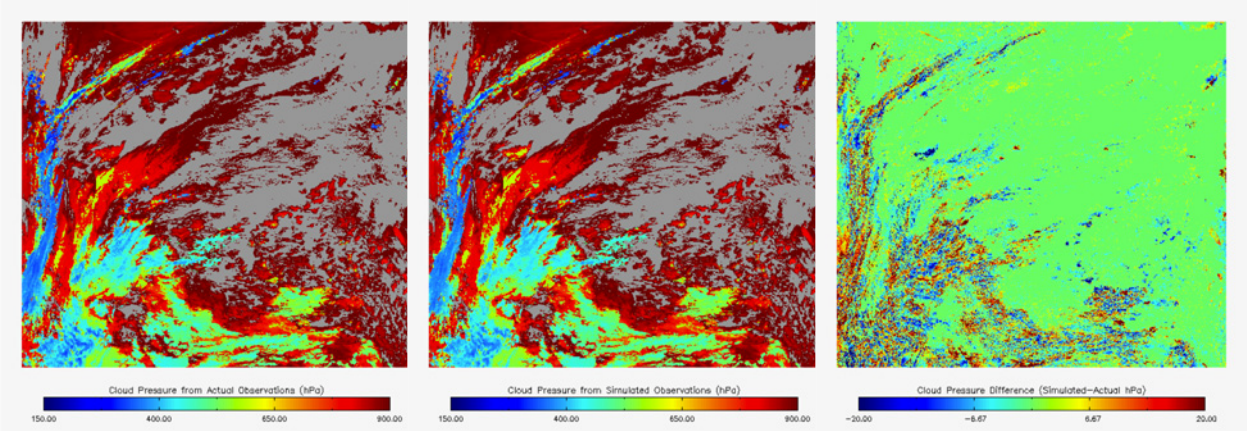

Figure 8: Cloud Top Pressure product: original 13.3 micron band (left) and estimated (middle), and difference (right). Case 1: MODIS Aqua granule MYD021KM.A2012020.0500.

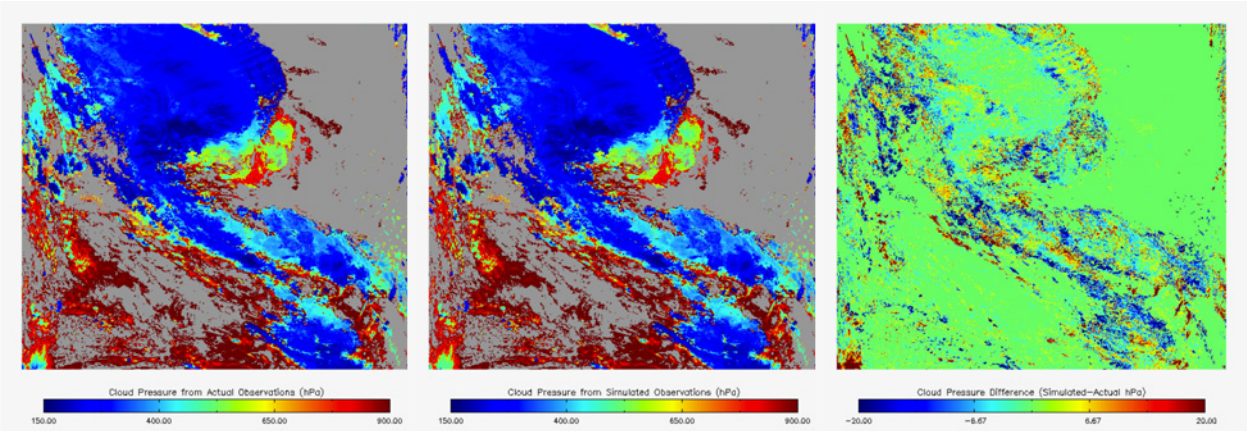

Figure 9: Cloud Top Pressure product: original 13.3 micron band (left) and estimated (middle), and difference (right). Case 2: MODIS Aqua granule MYD021KM.A2012243.0440.

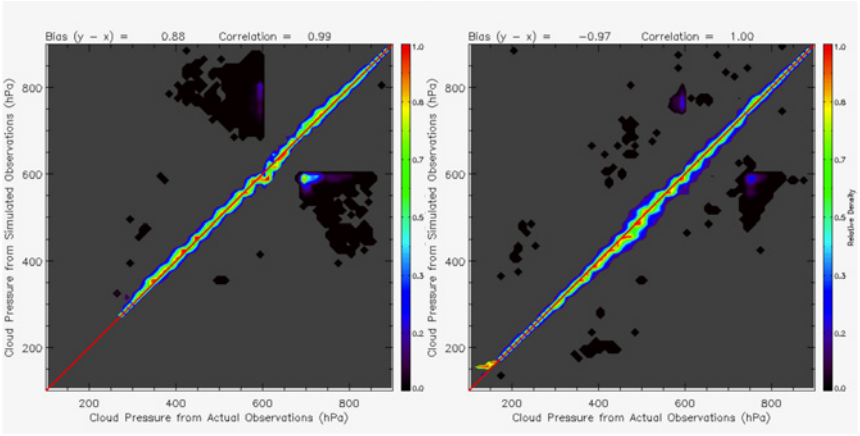

Figure 10: Scattergrams of Actual versus Synthesised 13.3 micron bands: Case 1 (left), Case 2 (right)

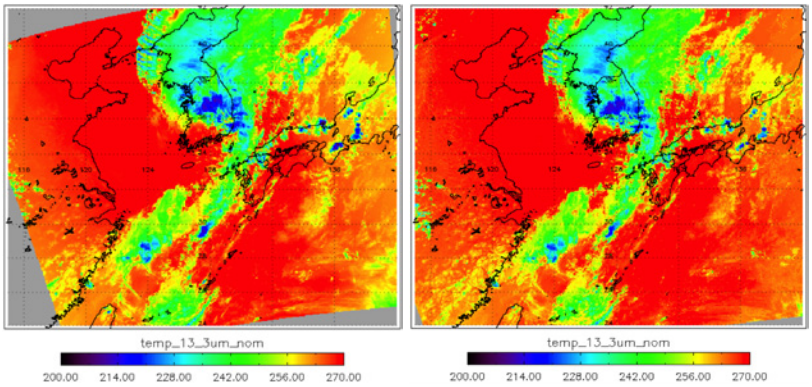

Figure 11: 28 August 2012 MODIS measured 13.3 micron brightness temperatures at 4:30 UTC (left) and VIIRS statistically reconstructed 13.3 micron brightness temperatures (right) at 4:40 UTC.

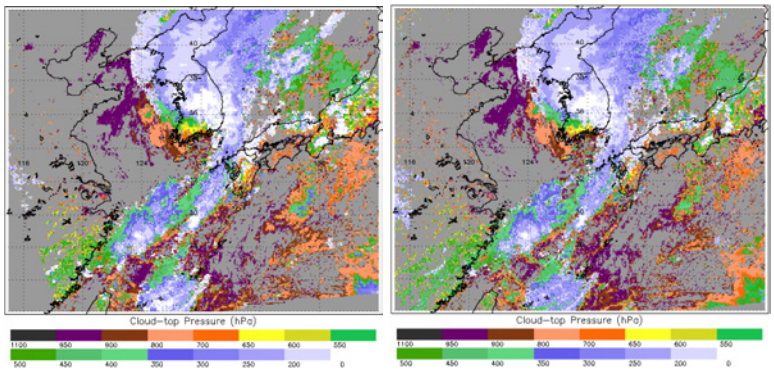

Figure 12: 28 August 2012 cloud top pressures derived using the ABI algorithm (left) from MODIS measurements at 04:30 UTC and (right) from VIIRS measurements and the statistically reconstructed from CrIS 13.3 micron channel at 04:40 UTC.

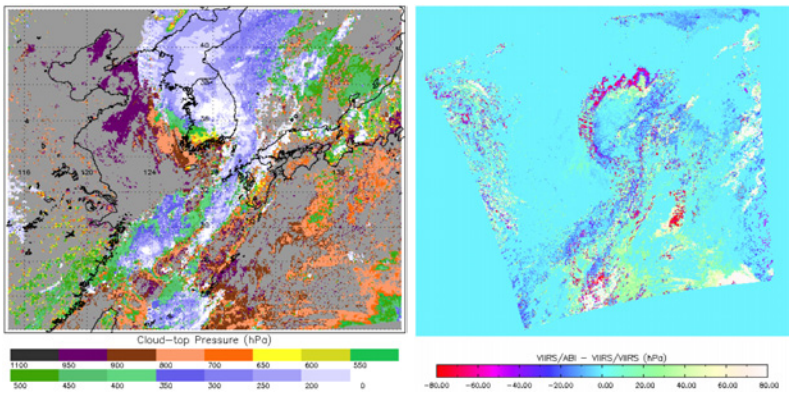

Figure 13: (left) 28 August 2012 cloud top pressures derived from VIIRS data without the 13.3 micron data using an optimal estimation approach that relies on the NCEP Global Data Assimilation System as a first guess. (right) Difference of CTPs with minus without 13.3 micron data.